NPL
National Physical Laboratory

NPL REPORT MS 5

Tools for Continuous Modelling Case Study 2: organic light-emitting diodes

Trevor Esward, Steven Knox, Louise Wright

November 2010

National
Measurement
System

NPL Report MS 5

Tools for Continuous Modelling Case Study 2: organic light-emitting diodes

Trevor Esward, Steven Knox, Louise Wright
Mathematics and Scientific Computing Group

November 2010

ABSTRACT

This report describes the application of sensitivity analysis and optimisation methods to a simulation of a dark injection transient current experiment on an organic light-emitting diode. The aim of the work was to calculate estimates of unknown properties by matching model predictions to measured data. The sensitivity and optimisation work builds on the results of earlier investigations reported in *Sensitivity analysis, optimisation, and sampling methods applied to continuous models* [6] and *Sensitivity analysis, optimisation, and sampling methods applied to continuous models: three test cases* [7].

NPL Report MS 5

ISSN 1754–2960

National Physical Laboratory,
Hampton Road, Teddington, Middlesex, United Kingdom TW11 0LW

We gratefully acknowledge the financial support of the UK Department for
Business, Innovation and Skills (National Measurement Office)

Approved on behalf of NPLML by Jonathan Williams,
Knowledge Leader for the Optical Technology and Scientific Computing team

Contents

1 Introduction

The case study reported here forms part of the Software Support for Metrology (SSfM) project "Tools for Continuous Modelling and Simulation". The aims of this project are to improve the understanding and use of continuous modelling packages and to improve the confidence of model users in the quality of their results. The case studies aim to illustrate the applicability of lessons learnt from the first stages of the project to solving real design problems.

The initial stages of the project compared a number of different sensitivity measures and different sampling and optimisation methods by applying them to three small finite element problems [7]. In addition to highlighting properties of each of the measures and methods tested, this initial work also identified valuable guidelines for developing an efficient methodology to apply to the case studies and to future work in this area [6].

There are two case studies that apply the methodology developed through the initial small test problems to real-world metrology problems. The case study presented in this report describes a model simulating the behaviour of organic light-emitting diodes (OLEDs). The aim of the work is to determine unknown properties of a device by matching model predictions to measurement data. The measurement data were gathered during dark injection transient current experiments. The experimental set-up used to obtain the data is described in section 2.

The model used to simulate the experiment is described in section 3, including the details of the objective function associated with the optimisation. Section 4 describes the process and results of an initial sensitivity analysis aiming to decide which parameters have the largest effect on the quality of the fit of the model results to the measured data. Section 5 describes a series of optimisations that aim to understand the effect of the different parameters and to find the most appropriate values for fitting under a variety of conditions. Finally section 6 identifies conclusions and general points that can be applied to optimisation of other similar models.

1.1 An introduction to charge transport

Electrical currents are caused by the flow of charge-carrying entities. In the most familiar models of charge transport the charge carriers are electrons (carrying a negative charge). It is also possible for a flow of "electron holes" to cause a current. If there is a gap in a molecular orbital, then an electron from an adjacent (full) molecular orbital can fill in the gap, effectively causing the gap to flow in the opposite direction. This idea is illustrated in figure 1. The black circles represent electrons, and the white circles represent gaps. The arrow represents the electron hopping into the gap, and the figure shows that although the elctrons move from

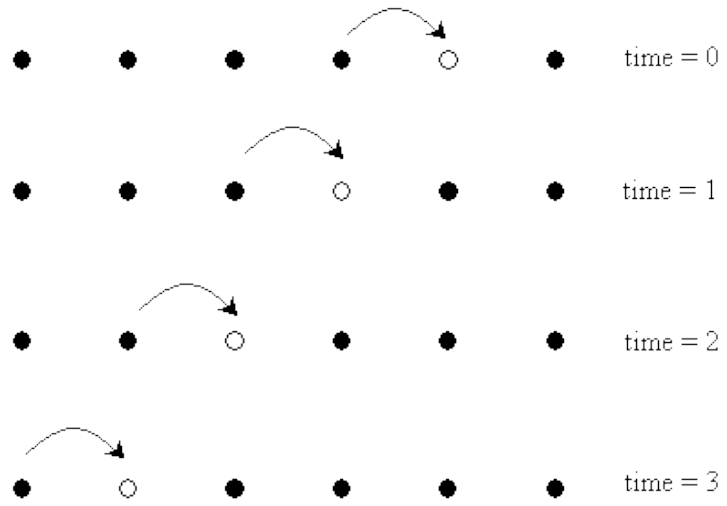

Figure 1: Illustration of how an electron hole can flow and cause a current as electrons move to fill the hole in. Black circles represent electrons, white circles represent the electron hole, and the arrows show the direction of motion of individual electrons.

left to right, the hole effectively moves from right to left. The device considered in the work reported here is a hole-only device, but devices (typically made of layers or mixtures of different materials) exist that involve the flow of both types of charge carrier.

Whilst electrons and holes are discrete objects, they are treated as continuous quantities in the work reported here. This approach uses the carrier density (in m^{-3}) to quantify how many electrons or holes there are at a given point. The approach results in a set of deterministic partial differential equations describing charge transport. Approaches that consider the motion of individual charge carriers usually result in a (very) large set of simultaneous stochastic equations whose statistics averaged over a large number of model runs provide a description of the charge transport.

The most common class of approaches that consider the motion of individual charge carriers is the family of hopping models. Hopping models assume that individual charge carriers move on a very large grid of points, and the probability of a carrier "hopping" or transferring to a nearby site is given by a set of stochastic equations. The law of charge conservation and Gauss' law are used to couple together the equations governing the motion of each carrier, the configuration of all the charge carriers is calculated at a number of timesteps, and the results are used to calculate currents. Recent work has shown [13, 19, 20] that for an appropriate choice of continuum model, hopping models and continuum models give the same results.

In the continuum approach, charge carrier motion is driven by two main processes:

drift driven by the local electric field and thermal diffusion. The electric field is caused by the applied voltage and the charge distribution within the device, so field and charge transport are closely coupled. The rate at which charge flows through a material is strongly dependent on the **mobility** of the charge carrier of interest, which is a property of the bulk material. The details of the equations describing these processes will be given in section 3.

Another process affecting the charge distribution is charge trapping. Traps can restrict the movement of the less energetic charge carriers. The trap properties of a material are defined as a **trap density** (in m^{-3}), a trap cross-sectional area (in m^2, and a **trap depth** (an energy typically defined in eV). Trapping is described in more detail in setion 3

The final factor considered here that affects charge carrier motion is how well the electrodes supply charge carriers to the device. An electrode that offers an effectively limitless supply of charge carriers to the device is known as an ohmic contact. The work reported here has included consideration of non-ohmic contacts, and has considered the **contact quality** by reducing the density of charge carriers available for injection.

1.2 Organic light-emitting diodes

Organic light-emitting diodes typically consist of a pair of electrodes, a substrate, and a conductive layer and an emissive layer that consist of organic molecules. The conductive layer transports holes, the emissive layer conducts electrons, and the electrons and holes combine close to the boundary between these two layers to form excitons. When the excitons decay they emit a photon with a frequency in the visible range. The use of organic molecules allows the substrates used to be thin and flexible, which significantly broadens the range of applications for LED technology.

The charge mobility of the electrons and holes within a device affect its performance since they affect the rate at which the electrons and holes can meet and combine to generate light. An understanding of the charge transport can lead to design of more efficient devices.

2 Experimental details

This section describes the experiment that generates the data and discusses the processing of the data to obtain the charge mobility.

2.1 Experimental procedure

The experiment simulated in the work reported here is called the dark injection transient current (DITC) experiment [15]. This experiment, and other similar space-charge limited transient current experiments, are used to investigate the charge transport properties of electronic devices. Space-charge limited means that an effectively infinite supply of charge carriers is available for injection into the device, and so the charge transport is governed by the characteristics of the device rather than those of the electrodes.

A simple description of the experiment is that the device of interest has at least one electrode that is ohmic for the charge carrier of interest (electrons or holes), and a step change in voltage is applied to the device. The time-dependent current response to the voltage step is measured. Analysis of this current response can give information about the charge transport properties of the device. The data analysis techniques will be discussed in more detail in section 2.2.

The implementation of the experiment used to generate the data used here is slightly more complicated. The main complication is that the applied voltage is not a simple step. Instead, the voltage is turned on, off, and on again, and the current measurement is taken during the second "on" period. The work reported here has used a 1 ms "on" period with both "on" periods being the same length, and an off period of 49 ms. Whilst experiments have been carried out with a range of voltage step sizes, the work reported here has used an 8 V step.

The voltage supply is an Agilent 81101A pulse generator, and the current measured is displayed on a Tektronix DPO4104 1 GHz oscilloscope. During the experiment the device of interest is mounted in a manner that thermally isolates the device and shields it from light since both heat and light can affect the device behaviour. The data as originally supplied are voltages taken from the oscilloscope, and these values are converted to current using the known internal resistance (100 Ω total) of the oscilloscope.

2.2 Data processing

The main output of the experiment is a measurement of the current through the device over time. If the device was trap-free with ohmic contacts between the main body of the device and the electrodes and no thermal diffusion, then the current measurement would resemble the lower curve shown in figure 2. In this figure, J_{SCL} is the space-charge limited current, given by Child's Law [8],

$$J_{SCL} = \frac{9\epsilon\mu V^2}{8L^3} \tag{1}$$

where ϵ is the permittivity of the material (relative permittivity of the material multiplied by permittivity of free space), μ is the charge mobility for the carrier of

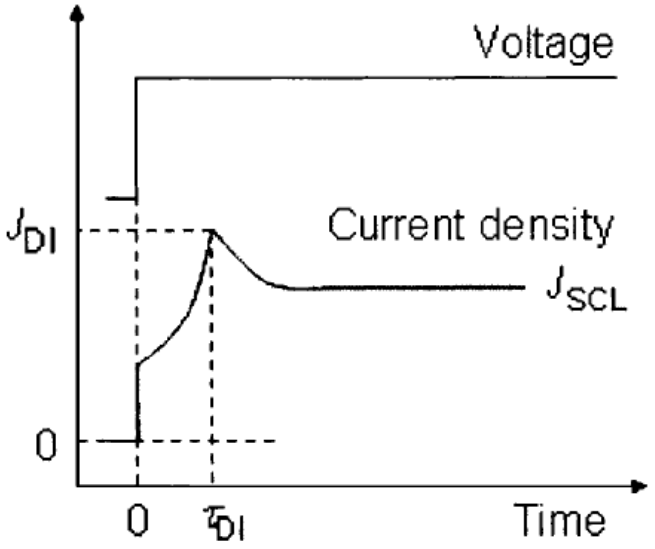

Figure 2: Idealised representation of experimental output

interest as mentioned in 1.1, V is the applied voltage and L is the thickness of the device in the direction of charge flow.

Analysis of a simplified form of the transient equations introduced in section 3 [8] shows that the peak current J_{DI} is given by

$$J_{DI} = \frac{\exp\{1\}\epsilon\mu V^2}{2L^3}, \tag{2}$$

and the time at which the peak occurs (τ_{DI}) is given by

$$\tau_{DI} = \frac{2(1-\exp\{-0.5\})L^2}{\mu V}. \tag{3}$$

Rearranging (3) to obtain an expression for the carrier mobility gives

$$\mu = \frac{2(1-\exp\{-0.5\})L^2}{\tau_{DI} V}. \tag{4}$$

and this expression is used to process DITC measurement data in order to obtain a mobility value.

The simplifications used to achieve these results are that the material is trap-free, that thermal effects are minimal, and that contacts are ohmic. These neglected phenomena affect the position, height, and sharpness of the peak shown in figure 2. A more typical data set is shown in figure 3, along with a close-up of the region used to determine an experimental value of τ_{DI}. This data set has been used throughout the work reported here. Applying (4) to the data, using $L = 205$ nm,

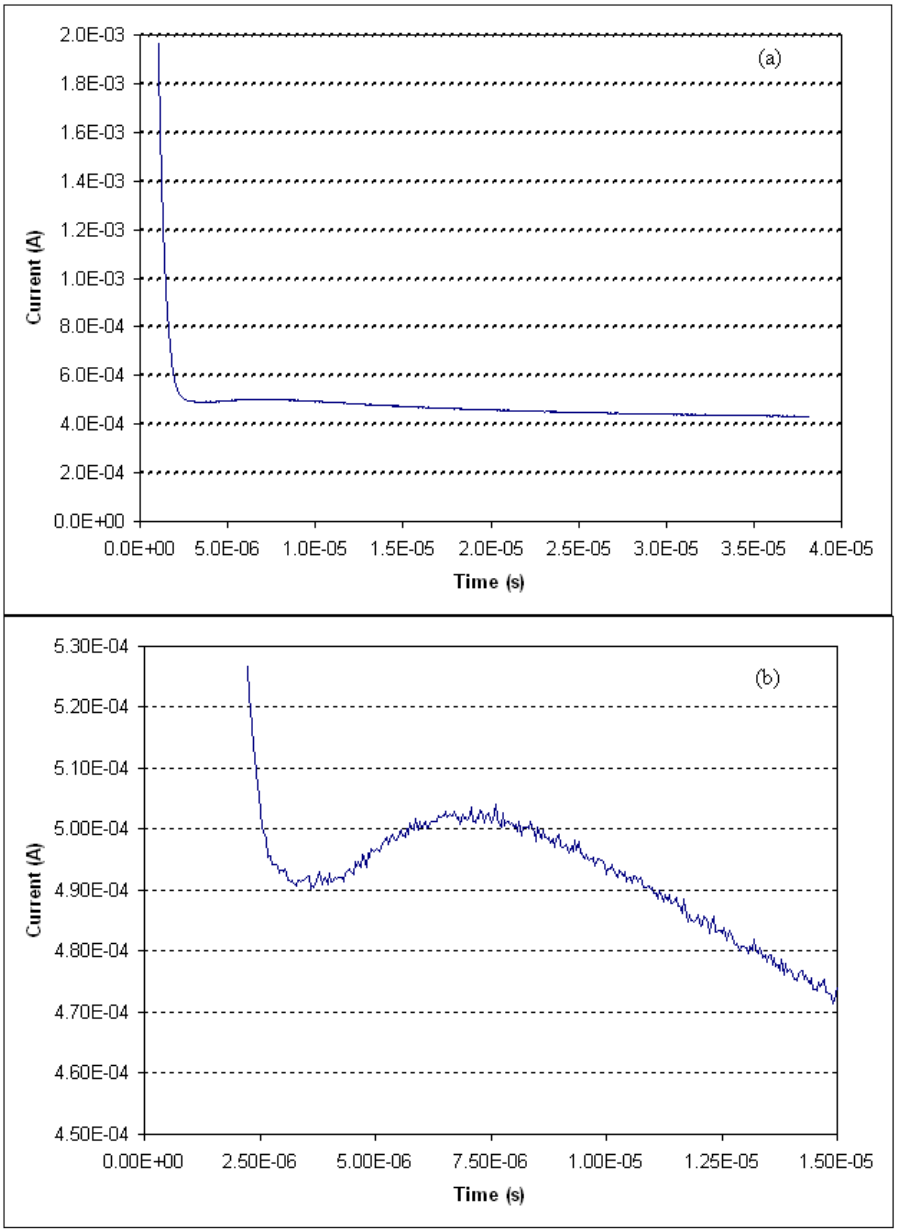

Figure 3: Full data set measured during the DITC experiment, (a), and a close-up of the data used to determine mobility using an analytical formula (b).

$V = 8$ V, and $\tau_{DI} = 6.9$ μs gives a value for the carrier mobility of $\mu = 5.96 \times 10^{-10}$ m^2 V^{-1}s^{-1}.

When the data were measured, a data point was taken every 4×10^{-8} s and the data shown were measured between 1.04×10^{-6} s and 3.824×10^{-5} s. Data points at the earliest times overloaded the oscilloscope and so these points have been omitted from the set shown. The data in figure 3 have been used as **target data** during subsequent optimisation calculations. The aim of the optimisation calculations was to minimise the difference between the target data and the calculated results by varying combinations of the model parameters.

3 Model details

This section defines the equations and boundary conditions that constitute the model and describes the numerical techniques used to solve the model.

3.1 Equations and boundary conditions

The model used in this work is based on that described in [18]. The device considered in the work reported here is made from a single uniform material and uses holes to transport charge. It is assumed that the device is sufficiently large and uniform in two directions that charge flow is only significant in the through-thickness direction and so a one-dimensional model can be used. It is assumed that all material properties are constant and uniform, and that there is no intrinsic charge density. It is assumed that the electrodes supplying the charge carriers can be modelled as boundary conditions rather than requiring a detailed model themselves.

The equations governing the charge transport are given by

$$\frac{\partial^2 \phi}{\partial x^2} = \frac{e(p_f + p_t)}{\epsilon}, \tag{5}$$

$$\frac{\partial p_f}{\partial t} = \mu \left(\frac{k_B T}{e} \frac{\partial^2 p_f}{\partial x^2} + \frac{\partial}{\partial x} \left\{ p_f \frac{\partial \phi}{\partial x} \right\} \right) - \frac{\partial p_t}{\partial t}, \tag{6}$$

$$\frac{\partial p_t}{\partial t} = \sigma_t \mu \left(\left\| \frac{\partial \phi}{\partial x} \right\| + \frac{k_B T}{e \Delta x} \right) \times \left[p_f (N_t - p_t) - p_t (N_{HOMO} - p_f) e^{-E_t/(k_B T)} \right] \tag{7}$$

where x is the spatial coordinate, $0 \leq x \leq L$, Δx is a small distance, t is time, and

- $\phi(x,t)$ is the electric potential,
- $p_f(x,t)$ and $p_t(x,t)$ are the densities of free and trapped holes, respectively,
- e is the charge on an electron, 1.602×10^{-19} C,

- μ and ϵ are respectively the charge mobility and the permittivity of the material, as in section 2.2,
- k_B is Boltzmann's constant, 1.38×10^{-23} J K^{-1},
- T is the temperature, assumed constant throughout,
- σ_t is the trap cross-sectional area,
- N_t and E_t are respectively the trap density and the trap depth as mentioned in section 1.1, and
- N_{HOMO} is the density of free states in the highest occupied molecular orbital (HOMO).

Equation (5) is Gauss' law. The three terms in equation (6) represent changes in the number of free charge carriers due to (left to right) thermal diffusion, field-driven drift, and trapping. Equation (7) shows that the trapping and detrapping depends on the trap area σ_t, and the velocity of the carriers at that point, approximated by

$$\mu \left(\left\| \frac{\partial \phi}{\partial x} \right\| + \frac{k_B T}{e \Delta x} \right). \tag{8}$$

The final bracketed term in equation (7) defines the amount of free holes that become trapped as depending on the density of free holes and the density of empty traps, and the amount of trapped holes that become free as depending on the density of trapped holes, the density of empty states for the free holes to pass into, and a term dependent on the energy state distribution of the holes.

The main result of interest from the model is the current j flowing through the device, given by

$$j(x,t) = Ae\mu \left(\frac{k_B T}{e} \frac{\partial p_f}{\partial x} + p_f \frac{\partial \phi}{\partial x} \right) \tag{9}$$

where A is the cross-sectional area of the device. Values of $j(L,t)$ are compared to the experimental data during the optimisation process, where L is the thickness of the device.

The boundary conditions on the potential are

$$\phi(0,t) = 0 \tag{10}$$
$$\phi(L,t) = V_S(t) - V_{bi} - V_R \tag{11}$$

$V_S(t)$ is the supply voltage, given by

$$V_S(t) = \begin{cases} V_{amp}, & 0 \le t \le t_{\mathtt{on}},\ t_{\mathtt{off}} + t_{\mathtt{on}} \le t \le t_{\mathtt{off}} + 2t_{\mathtt{on}}, \\ 0, & t_{\mathtt{off}} \le t < t_{\mathtt{off}} + t_{\mathtt{on}}, \end{cases} \tag{12}$$

where V_{amp} is the amplitude of the applied step voltage and $t_{\mathtt{on}}$ and $t_{\mathtt{off}}$ are respectively the on and off times described in section 2.1. V_{bi} is the built-in

potential, the potential difference across the device when it is in thermal equilibrium. V_R is a voltage that accounts for the resistances in the experimental equipment other than the device, and is given by $V_R = Rj(L,t)$ where R is the known resistance of the components other than the device. It is assumed that these components do not affect the availability of charge carriers for injection into the device.

The boundary conditions on the free carriers are that no thermal diffusion occurs into the device from the electrodes, that a large density p_{anode} of carriers is available to drift into the device at $x = 0$ and that the drift is controlled by the field at $x = 0$, and that nothing stops the drift of carriers out of the other electrode at $x = L$. These conditions neglect more complicated methods of charge transport such as tunneling. Additionally, any barriers to injection at the electrodes are not modelled directly. Instead their effects are simulated by reducing p_{anode}, thus allowing for non-ohmic contacts. It is not clear how to write these conditions as a function of the variables and their differentials and so this has not been attempted. The conditions have been implemented within the software in the manner suggested by Staudigel et al [18].

The trapped carriers do not need boundary conditions as their spatial derivative does not appear anywhere in the equations. It is assumed that at $t = 0$ there is zero electrical field and zero carrier density (trapped or untrapped).

3.2 Numerical solution technique and software implementation

The set of nonlinear coupled equations (5), (6) and (7) are too complicated to be solved analytically without further approximations and simplifications, so a numerical solution method must be used. The numerical technique used is based on that described in [18]. The technique applied in that paper applies conservation of charge to thin strips within an OLED to derive a set of coupled ordinary differential equations for free and trapped charge carrier density within the device, effectively applying a finite volume technique to equations (5), (6) and (7). The solution of this system of equations allows the transient behaviour of the charge carriers and the electric field to be calculated. The coupled set of ordinary differential equations have been solved using a variable order multistep solver based on the numerical differentiation formulas [16, 17]. A solver suitable for stiff equations has been used because it is not clear whether the equations would be stiff or not, but the different time scales over which the physical processes occur makes stiffness a possibility. The differential equations describe the behaviour of the charge distribution and the electric field can be calculated from the charge distribution using (5).

Various software packages are available that implement continuum models (see, for example, Fluxim, Atlas, and SimOLED), but creation of our own software has several advantages. As well as offering flexibility for further development and

complete control over the models and boundary conditions used, it makes running of batch jobs for sensitivity analysis and interfacing with optimisation routines considerably more simple. The work described here has been implemented within Matlab and makes use of its intrinsic routines for solution of ordinary differential equations, particularly `ode15s` which is designed to solve stiff systems.

The model requires a large number of inputs. In the work described here, the quantities μ (charge mobility), N_t (density of traps), E_t (trap depth), and p_{anode} (density of charge carriers at the anode) were regarded as parameters to be determined. The remaining inputs were fixed as follows:

- $L = 205 \times 10^{-9}$m (M),
- $\epsilon = 3.0 \times 10^{-11}$ F m^{-1} (M),
- $V_{bi} = 0.73$ V (M),
- $T_0 = 295$ K (E),
- $\sigma_t = 5 \times 10^{-18}$ m^2 (E),
- $N_{HOMO} = 10^{-27}$ m^{-3} (E),
- $V_{amp} = 8$ V (M),
- $R = 100\,\Omega$ (M),
- $A = 1.025 \times 10^{-5}$ m^2 (M),
- $t_{\mathtt{on}} = 10^{-3}$ s (M),
- $t_{\mathtt{off}} = 0.049$ s (M).

The quantities marked (M) were measured during the experiment or as a separate measurement of the device of interest. The quantities marked (E) were estimates, typically based on literature values. N_{HOMO} and σ_t were taken from [18].

The objective function for the optimisation procedure was chosen to be an unweighted root mean square of the relative differences between the measured and calculated values (differences relative to the measured values). This function can be written

$$f = \sqrt{\frac{1}{931}\sum_{n=1}^{931}\left(1 - \frac{j_{mod}(t_n; N_t, E_t, \mu, p_{anode})}{j_{meas}(t_n)}\right)^2}, \tag{13}$$

where $j_{mod}(t_n; N_t, E_t, \mu, p_{anode})$ is the model's calculated current at the cathode ($x = L$) at time t_n for a specific set of model parameter values and $j_{meas}(t_n)$ is the measured current at time t_n.

An unweighted mean was chosen because initially all parts of the data were regarded as being of equal importance. The relative difference was used because all

of the measured values were sufficiently far from zero that small absolute errors would not lead to large relative errors. No limits were placed on the parameters during the optimisation but during the initial sensitivity analysis μ was varied between 0 and 10^{-9} m^2 V^{-1} s^{-1}, p_{anode} was varied between 0 and 10^{26} m^{-3}, N_t was varied between 0 and 10^{24} m^{-3}, and E_t was varied between 0 and 0.7 eV (larger trap depths sometimes caused problems with the solution of the model). Literature values [1, 2, 3, 9] have suggested that the trap depth is less than 1 eV and the trap density is of the order of 10^{23} m^{-3}.

3.3 Validation and initial test

The implementation of the model was validated by comparing results of a trap-free device with no diffusion and ohmic contacts to the various expressions in [8], including the expression for the initial transient current. Agreement was sufficiently good that the model implementation was considered to be validated.

As a further initial comparison between the idealised model described in [8] and section 2.2, the value calculated for mobility from the data using the simplified approach was used in a trap-free version of the model with ohmic contacts. The calculated results are shown in figure 4. This figure illustrates that the values of τ_{DI} and J_{SCLC} are not consistent with one another, suggesting that the simplified model used in [8] is not suitable for describing real devices. A closer examination of the model results shows that the hump occurs at the right time, but the overall fit is very poor.

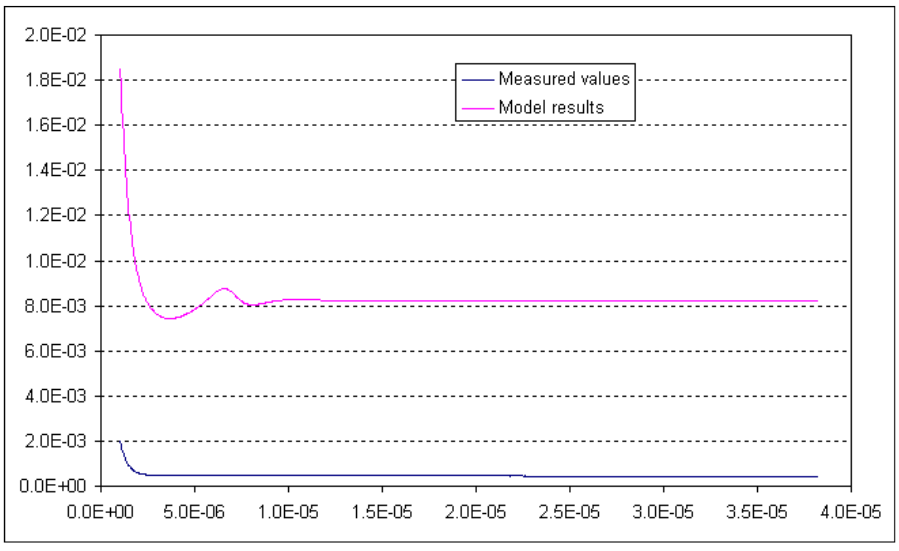

Figure 4: Results of the model using a mobility derived analytically from the experimental data, with ohmic contacts and no traps.

3.4 Limits and assumptions

Whilst the model described above is more complex than that used in [8], it still makes a number of assumptions about the device, and these will limit its applicability. The main assumptions are:

- The device is uniform in the directions parallel to its electrodes and can be accurately approximated by a one-dimensional model.
- The temperature is uniform and constant throughout the simulation.
- All material properties (permittivity, charge mobility, trap density, trap depth) are constant in time and uniform in space. In particular, field-dependent mobility has not yet been implemented.
- Intrinsic carrier density is zero.
- Charge carrier entry at the electrodes occurs through injection. Tunnelling is neglected, and so charge carriers only enter the device at the layers adjacent to the electrodes.
- The details of the energy states at the electrodes are not modelled directly. Any barriers to charge injection are modelled by reducing the number of charge carriers available for injection rather than by a detailed consideration of energy states.

4 Sensitivity analysis

A sensitivity analysis was carried out to investigate how the model parameters affected the value of the objective function. The Morris One-At-A-Time index [14] was used to compare the importance of the inputs. If the analysis showed that some of the parameters were more important than others then subsequent investigations would focus on the important parameters. An understanding of the objective function also allows for a more efficient choice of optimisation function. A rough surface with many local peaks is best tackled using a different algorithm to that which would be used for a smooth surface with a unique minimum. Visualisation of the results of a sensitivity analysis can also allow the user to get a clearer understanding of where the optimal solution is most likely to lie.

The sensitivity analysis used 880 model runs to calculate the index values for the input parameter values, generated from 176 groups of five runs each. Each group of runs produces one elementary effect for each input parameter. The indices calculated for each factor are the mean, standard deviation, and mean of absolute values of the elementary effects. A large mean value (in comparison with the mean of all function values) indicates that the model parameter has a strong effect on the function value. A large standard deviation means that a parameter is either having

a nonlinear effect on the function value or it is interacting with other parameters. If the mean of the absolute values is similar in size to the mean of the values, then the parameter's effect is largely monotonic. The calculated values are given in table 1. For comparison, the mean value of all the function evaluations was 6.36.

	N_t	E_t	μ	p_{anode}
Mean EE	-4.33	-15.8	11.4	0.64
S(EE)	7.86	14.3	11.9	1.77
Mean |EE|	4.45	15.9	11.4	0.73

Table 1: Mean, standard deviation (S) and mean absolute elementary effect (EE) for the model parameters trap density N_t, trap depth E_t, carrier mobility μ, and contact quality p_{anode}.

These values suggest that whilst all four parameters have some effect on the function value, the most important parameters are the trap depth and the carrier mobility. The standard deviations and mean of absolutes suggest that all parameters have a nearly monotonic nonlinear effect. An illustration of this is shown in figure 5. The colour of the points in the figure are determined by the function value and the axes are the trap depth and the carrier mobility. The function value varies fairly smoothly with the two parameters, with points in close proximity being generally similar in function value. This smoothness suggests that the other factors do not have a large effect on the function value, with some exceptions. The exceptions form local minima or maxima that could cause problems for some optimisation algorithms.

Some combinations of parameter values lead to a zero or near-zero value of j_{mod} for all times (in particular a low value of p_{anode} leads to low currents), and hence an objective function value of 1. It is expected that the optimal set of parameter values will lead to a function value of less than 1. A version of figure 5 with the colour axis focussed on the range [0,1] is shown in figure 6. This figure suggests that at a smaller scale, the surface is considerably less smooth and the other parameters have an effect on function value. Whilst these figures identify the most important parameters and show the global dependency of the objective function on the parameters, they do not give a particularly good indication of a good starting guess for the parameter values.

5 Optimisation

The roughness of the surface shown in figure 6 suggests that it would be of interest to attempt to find values for all four model parameters using an optimisation algorithm suitable for challenging problems. In addition to carrying out

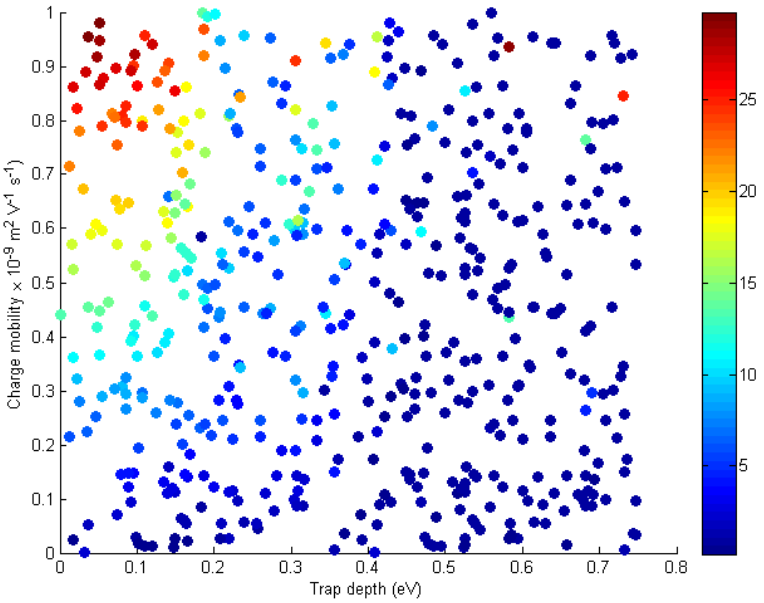

Figure 5: Function value (colour scale) plotted against trap depth and contact quality.

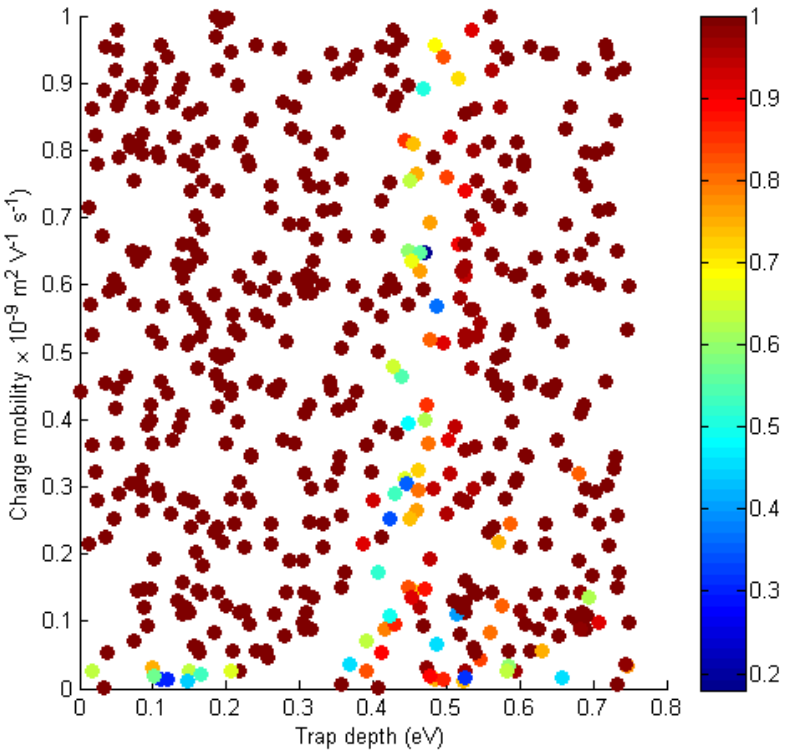

Figure 6: Figure 5 with a colour scale focussing on function values less than 1.

optimisations involving all four variables, a series of optimisations involving subsets of the model parameters were carried out to investigate the effects of the different features of the model (traps and non-ohmic contacts).

All optimisations were carried out using a simulated annealing [10] algorithm. Simulated annealing is a metaheuristic search algorithm that is particularly well-suited to optimisation problems involving discontinuous functions and those that have multiple local minima. In some cases, particularly for optimisations that only varied one parameter, this may not be the most efficient choice, but it was necessary for the optimisation involving all four parameters due to the surface roughness. In all cases the optimisation was started from a randomly-generated initial guess at the parameter values. The algorithm was only run once in each case. Metaheuristic algorithms generally search throughout the space of parameters and so a single run may be enough to identify a good solution. The time required for optimisation runs using simulated annealing meant that multiple runs were not feasible.

Initially an attempt was made to improve the fit of the simplest possible model (no traps, ohmic contacts) to the data. The values of N_t and E_t were set to zero and the value of p_{anode} was set to 10^{25} m^{-3}. The optimisation algorithm took 3961 function evaluations and obtained a value of $\mu = 6 \times 10^{-13}$ m^2 V^{-1}s^{-1}, a much smaller value than would be expected. The corresponding model results are shown in figure 7, along with the measured data. The results show that the current is a nearly linear function of time, that the expected bump does not occur within the timeframe of the measured results, but the final current is a better approximation to the measured value than that shown in figure 4. These results suggest that some of the assumptions made in the derivation of the analytical formula in [8] do not apply to the measured OLED.

The first assumption to be investigated was that of ohmic contacts. Instead of fixing p_{anode}, the value was allowed to vary during the optimisation, along with the mobility μ. The algorithm took 2591 evaluations of the model to converge. The best fit values found were $\mu = 2 \times 10^{-11}$ m^2 V^{-1}s^{-1} and $p_{anode} = 9.3 \times 10^{25}$ m^{-3}. The corresponding model results are shown in figure 8. The charge mobility is now sufficiently large that the bump occurs within the time frame of the results. Whilst the fit is an improvement, the model results still do not capture the key features of the experimental data in a satisfactory manner.

To investigate whether simulation of the presence of traps could improve the quality of the fit, an optimisation run was carried out that allowed the trap density N_t and trap depth E_t to vary whilst keeping the mobility fixed at $\mu = 5.96 \times 10^{-10}$ m^2 V^{-1}s^{-1} (the value calculated in section 2.2 and assuming ohmic contacts ($p_{anode} = 10^{25}$ m^{-3}). The optimal values were found to be $N_t = 8.2 \times 10^{22}$ m^{-3} and $E_t = 0.56$ eV, after 4156 function evaluations. Comparison of these values with literature values for similar materials [1, 2, 3, 9] suggests that the trap density and depth are both reasonable values. The results of the model using these values

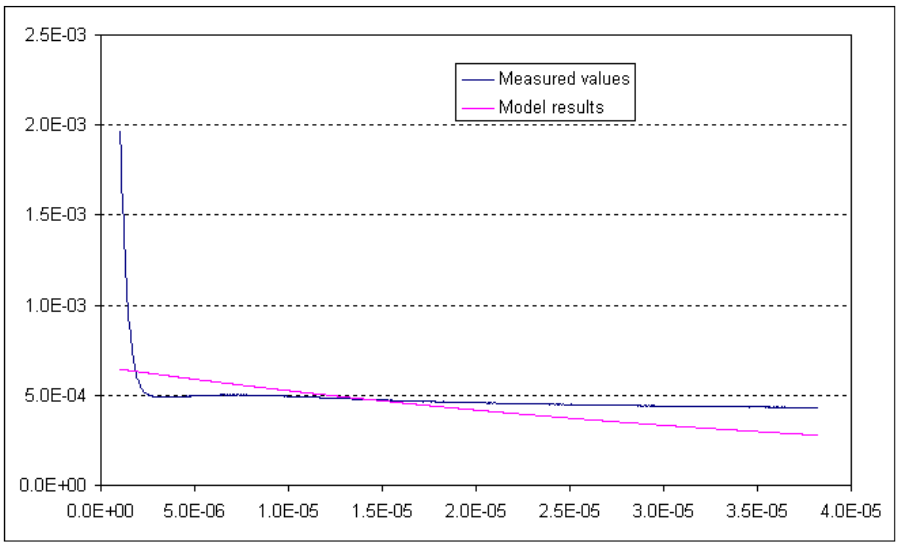

Figure 7: Results of the model using a mobility calculated by an optimisation algorithm, with ohmic contacts and no traps.

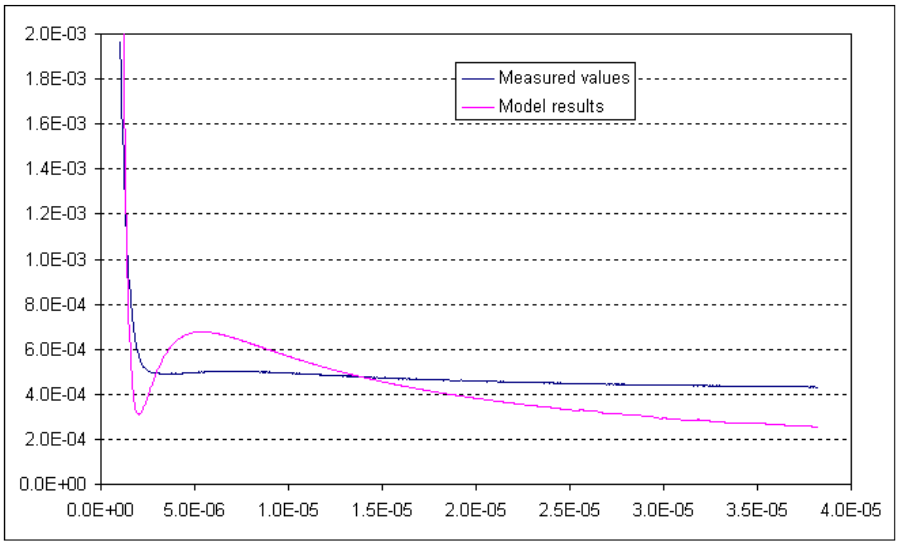

Figure 8: Results of the model using values of mobility and contact quality calculated by an optimisation algorithm, with no traps.

are shown in figure 9. These results show a good fit to the measured values at later times. The improvement suggests that the real system includes traps, and suggests that an optimisation involving all four variables could lead to further improvement as the interactions between parameters would then be taken into account.

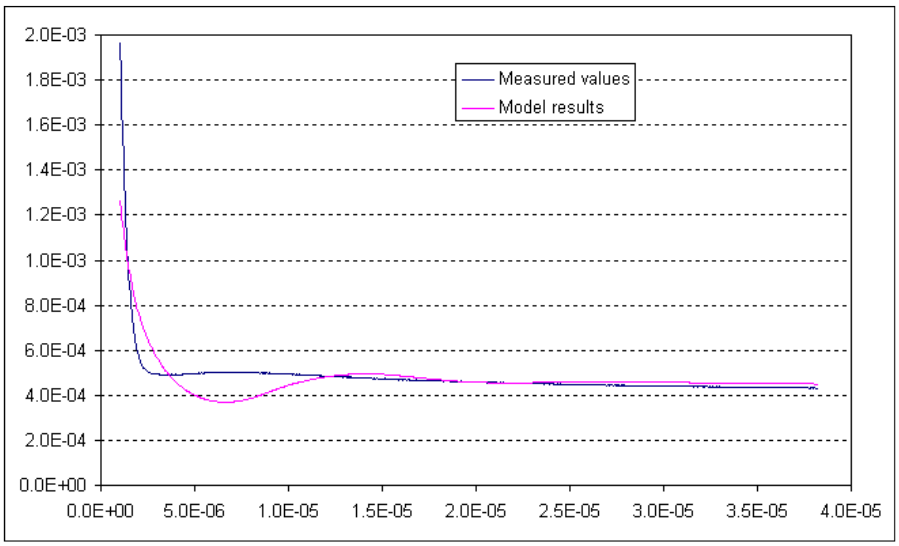

Figure 9: Results of the model using values of trap density and trap depth calculated by an optimisation algorithm, with ohmic contacts and fixed mobility.

The optimisation run using all four parameters led to the results shown in figure 10. The calculated optimal parameter values were $N_t = 8.1 \times 10^{22}$ m^{-3}, $E_t = 2.5$ eV, $p_{anode} = 5.6 \times 10^{25}$ m^{-3}, and $\mu = 5.98 \times 10^{-10}$ m^2 V^{-1}s^{-1}. These values were found after 6274 function evaluations. The fit is not very different from the fit shown in figure 9. This similarity is unsurprising because the charge mobility and trap density are similar to those used in generating figure 9, and the contacts are effectively ohmic.

The hump in the model results still occurs slightly later than that in the experimental data, but the current at later times agrees well with the measured values. Note that the value of the charge mobility is not significantly different from that determined using the standard data processing technique.

The plots shown in figures 10 and 9 differ only slightly, as do the values of N_t and μ used to calculate the plotted values. The value of p_{anode} used to calculate the curve shown in figure 10 is sufficiently large that the contact can be consered as ohmic and the contacts in 9 were treated as ohmic. The values of E_t used to calculate the plotted values differ sharply between the two plots, however, and the trap depth found during the optimisation of all four values is larger than has been reported for other similar materials [1, 2, 3, 9]. The small difference in fit between

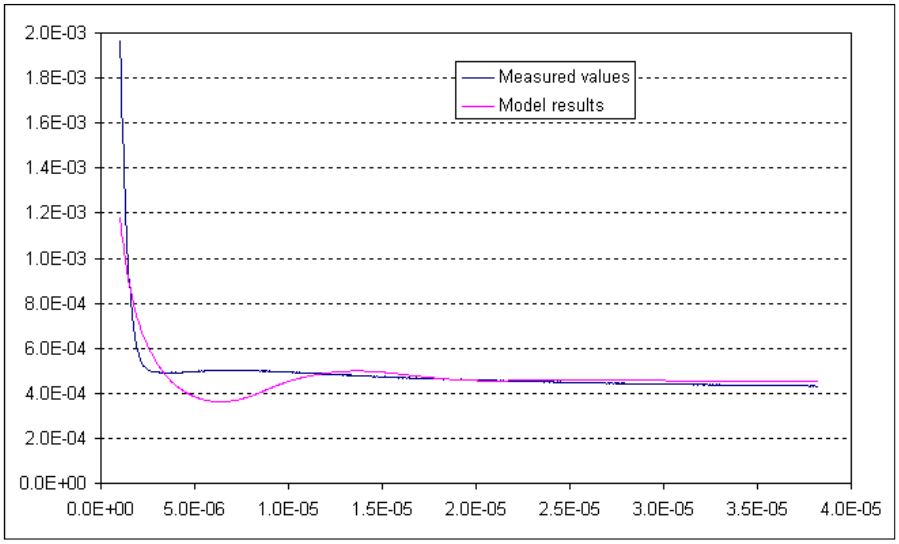

Figure 10: Results of the model using values of mobility, contact quality, trap density and trap depth calculated by an optimisation algorithm.

the curves and the large difference in trap depths suggests that whilst the trap depth is an important parameter globally for the objective function, it is less important in the direct vicinity of the optimal value.

This claim is highlighted by the plots shown in figure 11. This figure combines the results of the models evaluated during the optimisation runs to find just the trap parameters (shown as full blue squares) and those evaluated during the optimisation run to find all four parameters (shown as hollow pink circles). The runs to find the trap parameters used $\mu = 5.96 \times 10^{-10}$ m^2 V^{-1}s^{-1} and $p_{anode} = 10^{25}$ m^{-3}.

Figure 11(a) shows the dependence of the objective function value on the trap density. The curve has a well-defined sharp minimum, and the value of trap density at which the minimum occurs is independent of whether contact quality and charge mobility are allowed to vary or not. Figure 11(b) shows the dependence of the objective function on the trap depth. The curve is much flatter at the bottom, suggesting that the trap depth has less effect on the function value than the trap density. The fact that the minimum values for trap depths less than 2 eV are all from the "trap parameters only" optimisation run suggests that the optimisation on all four parameters did not search this region of the parameter space.

The parameter values found during each optimisation run are summarised in table 2, including the function value for the optimal parameter values. If a parameter was not varied during a particular run its value was fixed as follows: $N_t = 0$ m^{-3}, $E_t = 0$ eV, $\mu = 5.96 \times 10^{-10}$ m^2 V^{-1}s^{-1} and $p_{anode} = 10^{25}$ m^{-3}.

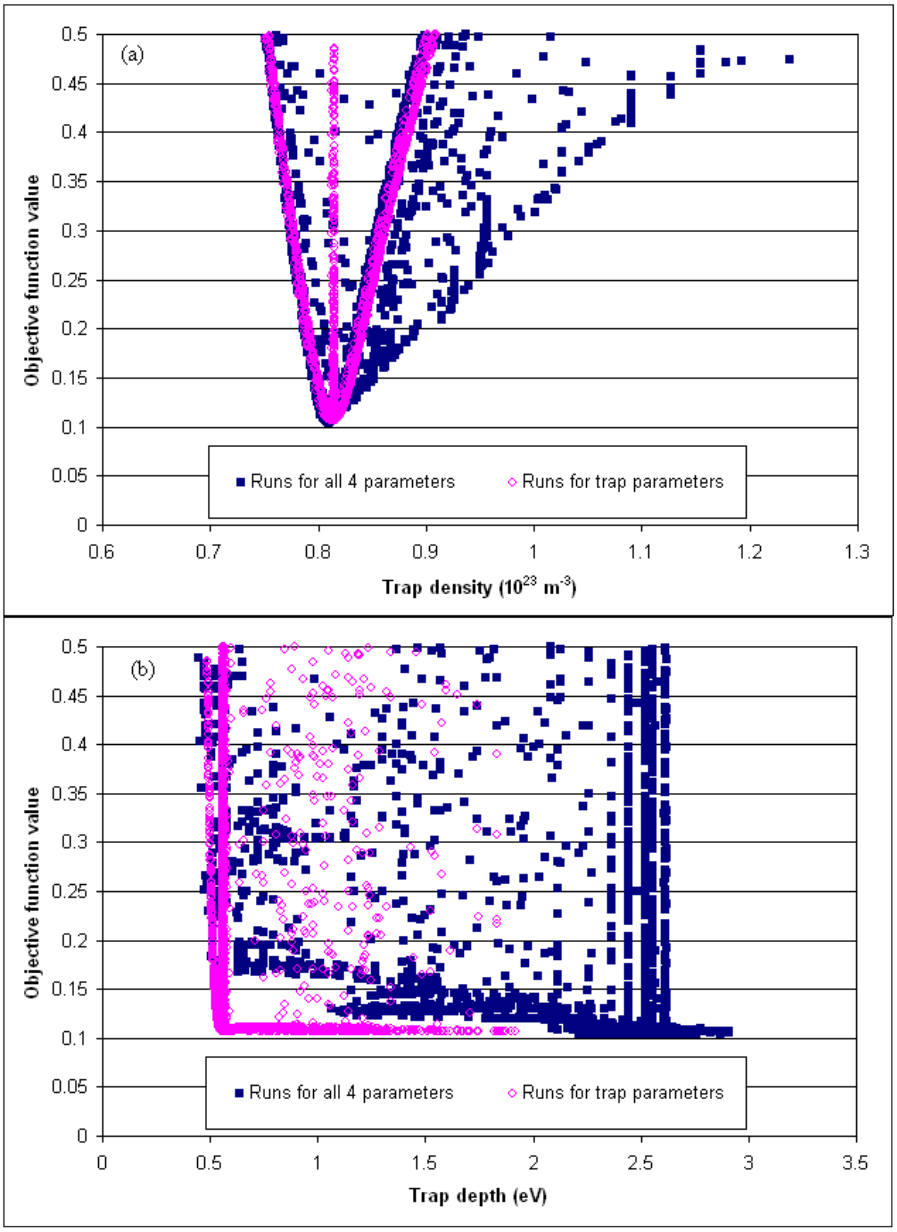

Figure 11: Objective function values less than 0.5 plotted against (a) trap density and (b) trap depth.

Run description	N_t (m^{-3})	E_t (eV)	p_{anode} (m^{-3})	μ ($m^2\ V^{-1}s^{-1}$)	Function value
Mobility	-	-	-	6×10^{-13}	0.20
Contact & mobility	-	-	9.3×10^{25}	2×10^{-11}	0.27
Trap parameters	8.2×10^{22}	0.56	-	-	0.11
All parameters	8.1×10^{22}	2.5	5.6×10^{25}	5.98×10^{-10}	0.10

Table 2: Summary of the optimal parameter values and minimal function values found during each optimisation run.

5.1 Alternative optimisation algorithms

In previous optimisation work (see *Sensitivity analysis, optimisation, and sampling methods applied to continuous models: three test cases*), the algorithm that performed best on the majority of test problems was the Matlab algorithm `lsqnonlin`. This algorithm is an implementation of the Levenburg-Marquardt algorithm [4, 5] designed to minimise functions that are sums of squares, such as that in (13). The algorithm is particularly effective when the objective function is smooth and unimodal. In general it requires significantly fewer model evaluations to reach a converged solution than other algorithms. The algorithm estimates local derivatives using finite differences and uses the estimates to determine its next search direction.

Figure 5 suggests that the surface is seemingly smooth at the plotted scale, and so the optimisation runs were repeated using `lsqnonlin`. Each of the optimisations outlined above was run 48 times starting from randomly-generated initial guesses. The results are shown in table 3. In this table, "converged function value" means the smallest function value that a given run of the `lsqnonlin` algorithm identified, and the average and minimum values are calculated over all 48 runs so the minimum converged function value was the best value that `lsqnonlin` found during its runs. The "distance" in the table is

$$\sqrt{\sum_{i=1}^{M}(x_i^0 - x_i^N)^2}, \tag{14}$$

where the x_i are the M model parameters allowed to vary in each optimisation after rescaling such that the starting guesses lie between 0 and 1, and x_i^0 is the initial guess at a parameter value and x_i^N is the converged value of the parameter. "Average func evals" means the average number of function evaluations before the algorithm reached a converged value.

The results are not good. The algorithm did not repeatedly converge to the same minimum solution, and many of the converged solutions were a long way from the minimum found by simulated annealing. In general the search did not move far from the starting guess, illustrated by low values of distance. The only way in

Run description	Converged function value			Average distance	Average func evals
	Average	Minimum	St dev		
Mobility	1.76	0.20	0.61	0.074	19
Contact & mobility	0.80	0.10	0.87	1.2	42
Trap parameters	10.3	0.22	6.4	1.2×10^{-5}	55
All parameters	1.27	0.18	0.56	0.26	39

Table 3: Summary of the performance of the `lsqnonlin` algorithm.

which `lsqnonlin` outperformed simulated annealing was that it found a lower minimum for the minimisation of p_{anode} and μ. A scatter plot of the response surface from the data gathered in all optimisation runs is shown in figure 12, which shows two regions of minimal function values: one with $p_{anode} \approx 10^{26}$ and $\mu \approx 0.2 \times 10^{-10}$ m^2 V^{-1}s^{-1} and a longer diagonal line in the middle of the plot. The first of these minima is local, and is the value that the simulated annealing algorithm found. The second valley minimum was found by `lsqnonlin`. If a sensitivity analysis had been carried out on this optimisation, this structure would have been known and an improved initial guess could have been used.

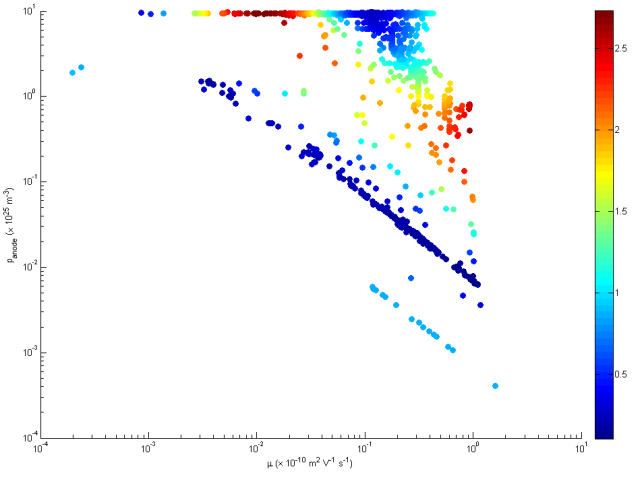

Figure 12: Objective function values from optimisation runs to identify μ and p_{anode} for a trap-free device shown as a scatter plot. Note the logarithmic scales on the axes.

The most likely reasons for the poor performance are local surface roughness and local minima. This possibility is backed up by analysis of a typical run. The plot in figure 13 shows the response surface of the optimisation involving the charge mobility determined from the simulated annealing runs. Note the logarithmic scale

on the horizontal axis. The curve has two minima, one global at about 6×10^{-13} m^2 $V^{-1}s^{-1}$ and one local at about 0.35×10^{-10} m^2 $V^{-1}s^{-1}$. Of the 48 optimisation runs carried out, 5 reached the global minimum and 23 reached the local minimum. Most, but not all, of the runs that had an initial guess of less than 0.1 $\times 10^{-10}$ m^2 $V^{-1}s^{-1}$ reached the global minimum. Figure 14 plots the initial guess against the final converged value, and shows that a small change in starting conditions can make a large difference to the converged value. This sensitivity suggests a locally rough surface. As an example, consider the values shown in figure 15. The plot is a close-up on one area of the function and shows a spike that would stop an optimisation algorithm reaching either of the two minima shown in 13. This local roughness is more likely to occur as the number of variables increases, but it is more difficult to identify and visualise in many dimensions. The local roughness and the existence of multiple minima explain why simulated annealing has generally been more successful that `lsqnonlin`.

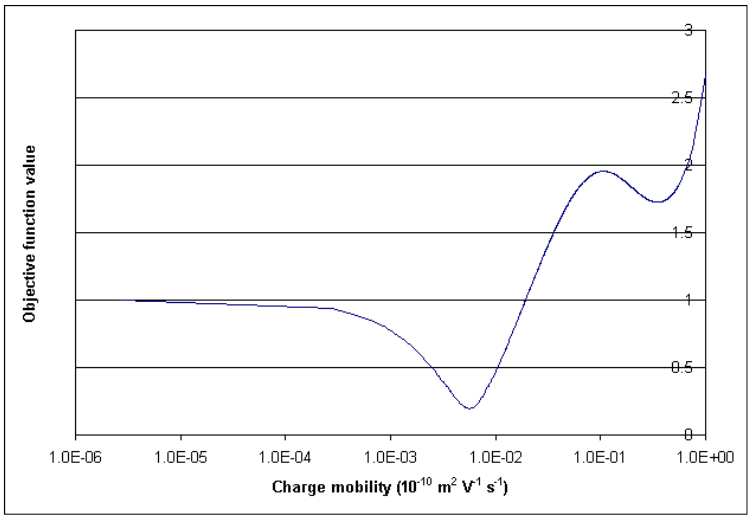

Figure 13: Objective function values from optimisation runs to identify μ for a trap-free device with ohmic contacts. Note the logarithmic scale on the horizontal axis.

The original intention had been to assign uncertainties to the parameter estimates by using sampling methods, but the difference between the predicted and measured values is not sufficiently good for that to be possible. The model as it stands does not describe the device sufficiently well for uncertainties to be associated with the model results. Implementation of more complicated models could lead to an improved description. It is likely that an improved fit could be obtained by allowing the carrier mobility to depend on the electric field as is commonly implemented within models of semiconductor devices. Variation of the trap properties with space may also improve the fit. The more complicated

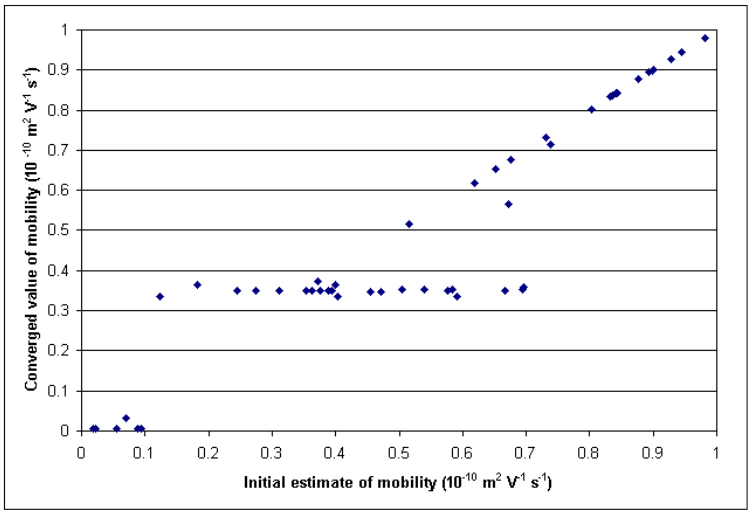

Figure 14: Initial estimate of charge mobility μ plotted against optimial value as identified by the algorithm `lsqnonlin`.

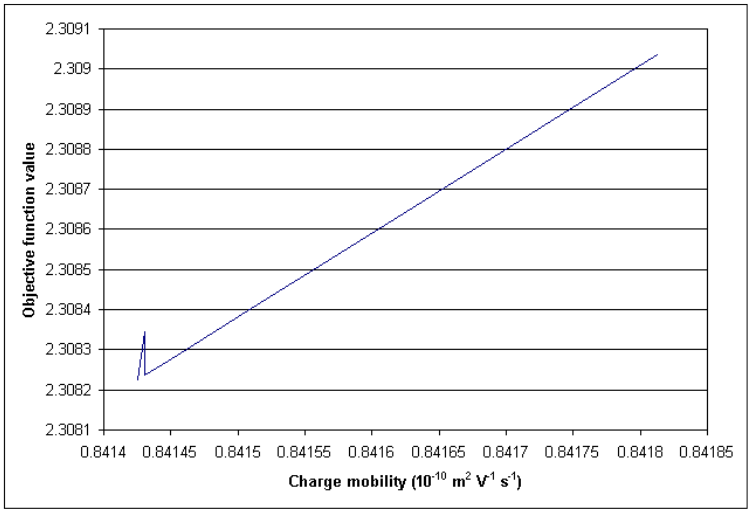

Figure 15: Plot of a small part of the curve shown in figure 13 showing local roughness.

boundary conditions, such as tunnelling of carriers, could be added to the model.

6 Conclusions

The work reported here has used optimisation techniques to try to determine the unknown properties of an organic light-emitting diode. The key points that are of general applicability are:

- The use of a sensitivity analysis has enabled the identification of the most important parameters of the model.
- The visualisation of the surface of the objective function at a suitable scale showed local roughness, making the choice of optimisation algorithm more straightforward.
- The use of optimisation techniques to find the best fit values for different combinations of parameters has shown how the inclusion of new details (traps and non-ohmic contacts) can improve the fit to the data.
- The use of a global optimisation algorithm (simulated annealing) has meant that the roughness of the surface has not affected the optimisation. Attempts to use a local optimisation algorithm have failed, even close to the minimum found by simulated annealing.

The model does not capture all of the physical processes that are occurring. The next step is to implement field-dependent mobility and apply the same optimisation techniques to determine parameter values.

References

[1] M. Arif, M. Yun, S. Gangopadhyay, K. Ghosh, L. Fadiga, F. Galbrecht, U. Scherf and S. Guha (2007) Polyfluorene as a model system for space-charge-limited conduction *Physical review B*, **75**, 195202.

[2] W. Brutting, E. Buchwald, G. Egerer, M. Meier, K. Zuleeg, M. Schwoerer (1997) Charge carrier injection and transport in PPV light emitting devices *Synthetic Metals*, **84**, 677-678.

[3] A. J. Campbell, D. D. C. Bradley, E. Werner and W. Brütting (2000) Transient capacitance measurements of the transport and trap state distributions in a conjugated polymer *Organic Electronics*, **1**, 21-26.

[4] T. F. Coleman and Y. Li. (1996) An interior trust region approach for nonlinear minimization subject to bounds. *SIAM Journal on Optimization*, **6** 418–485.

[5] T. F. Coleman and Y. Li. (1994) On the convergence of reflective newton methods for large-scale nonlinear minimization subject to bounds. *Mathematical Programming*, **67** 189–224.

[6] T. J. Esward, C. E. Matthews, L. Wright, X.-S. Yang. Sensitivity analysis, optimisation, and sampling methods applied to continuous models. NPL Report MS 2, NPL, 2010.

[7] T. J. Esward, C. E. Matthews, L. Wright, X.-S. Yang. Sensitivity analysis, optimisation, and sampling methods applied to continuous models: three test cases. NPL Report MS 3, NPL, 2010.

[8] W. Helfrich and P. Mark (1962) Space charge limited currents in anthracene as a method for the determination of the mobility of defect electrons *Z. Phys. (Germany)*,**166(4)**, 370-385.

[9] A. Kadashchuk, R. Schmechel, H. von Seggern, U. Scherf and A. Vaknin (2005) Charge-carrier trapping in polyfluorene-type conjugated polymers *Journal of Applied Physics*, **98**, 024101.

[10] S. Kirkpatrick, C. D. Gellat and M. P. Vecchi (1983) Optimisation by simulated annealing *Science*, **220**, 671-680.

[11] M. A. Lampert and P. Mark (1970) *Current Injection in Solids*, Academic Press.

[12] N.F. Mott and R.W. Gurney (1940) *Electronic Processes in Ionic Crystals*, Clarendon Press.

[13] W. F. Pasveer, J. Cottaar, C. Tanase, R. Coehoorn, P. A. Bobbert, P. W. M. Blom, D. M. de Leeuw and M. A. J. Michels (2005) *Phys.Rev. Lett*, **94**, 206601.

[14] A. Saltelli, K. Chan, and E. M. Scott. *Sensitivity Analysis*. Wiley, 2001.

[15] J. C. Scott, S. Ramos and G. G. Malliaras (1999) Transient space-charge-limited current measurements of mobility in a luminescent polymer *Journal of Imaging Science and Technology* **43**, 233-236.

[16] L. F. Shampine and M. W. Reichelt (1997) The MATLAB ODE Suite *SIAM Journal on Scientific Computing*, **18** 1-22.

[17] L. F. Shampine, M. W. Reichelt and J. A. Kierzenka (1999) Solving Index-1 DAEs in MATLAB and Simulink *SIAM Review*, **41**, 538-552.

[18] J. Staudigel, M. Stößel, F. Steuber and J. Simmerer (1999) A quantitative numerical model of multilayer vapor-deposited organic light emitting diodes *Journal of Applied Physics* **86(7)**, 3895-3910.

[19] S. L. M. van Mensfoort, and R. Coehoorn (2008) Effect of Gaussian disorder on the voltage dependence of the current density in sandwich-type devices based on organic semiconductors *Phys Rev B*, **78**, 085207.

[20] S. L. M. van Mensfoort, S. I. E. Vulto, R. A. J. Janssen, and R. Coehoorn (2008) Hole transport in polyfluourene-based sandwich-type devices: Quantitative analysis of the role of energetic disorder *Phys Rev B*, **78**, 085208.